Catalysis Today 447 (2025) 115146

Contents lists available at ScienceDirect

Catalysis Today

journal homepage: www.elsevier.com/locate/cattod

Zr-doped phosphorus-containing activating carbons catalysts for the valorization of furfural into valuables products in one-pot reaction

Rocío Maderuelo-Solera [a,b], Francisco José García-Mateos [c], Gabriela Rodríguez-Carballo [a,b], Cristina García-Sancho [a,b], Juana María Rosas [c], Ramón Moreno-Tost [a,b], José Rodríguez-Mirasol [c], Tomás Cordero [c], Pedro Maireles-Torres [a,b], Juan Antonio Cecilia [a,b,*]

[a] Departamento de Química Inorgánica, Cristalografía y Mineralogía, Facultad de Ciencias, Universidad de Málaga, Campus de Teatinos, Málaga 29071, Spain
[b] Instituto de Investigación en Biorrefinerías "I3B", Universidad de Málaga, Facultad de Ciencias, Campus de Teatinos s/n 29071, Málaga, Spain
[c] Departamento de Ingeniería Química, Facultad de Ciencias, Universidad de Málaga, Campus de Teatinos, Málaga 29071, Spain

ARTICLE INFO

Keywords:
Furfural
One-pot reaction
Activated carbon
Lewis/Brönsted acid sites

ABSTRACT

Olive stones have been used to synthesize activated carbon using H_3PO_4 as activating agent under pyrolytic treatment. Then, Zr species have been incorporated by impregnation and subsequent calcination, obtaining acid catalysts with Lewis and Brønsted sites, which are involved in the one-pot reaction of furfural in value-added products. All catalysts display a high micro- and mesoporosity. The catalysts showed different behavior as a function of the temperature, obtaining full conversion after 24 hours at 110 ºC, being mainly selective towards furfuryl alcohol and i-propyl furfuryl ether. The study at higher temperature (170 ºC) reached the full conversion after only 45 minutes, being preferentially selective towards i-propyl levulinate and γ-valerolactone. The catalysts are prone to suffer deactivation processes due to the formation of humins on the surface of the catalysts, which cause a decrease of the available active sites.

1. Introduction

In the last decades, the growing in world population and energy consumption have caused a decrease in levels of fossil resources. In the same way, many governments are carrying out more restrictive environmental legislation, which has led to the search and development of alternative energy sources, fuels and chemicals to replace fossil-based analogues sustainably.

Among the possible sources, biomass has a great potential to obtain energy but also chemicals, so biomass has shown great interest to the scientific community and companies to obtain compounds, which are generally obtained from the petrochemical industry. Amongst the possible sustainable resources, much attention is being paid to lignocellulosic biomass due to it is considered a widely available source, being non-edible in many cases. Lignocellulose is mainly composed by three components (hemicellulose, cellulose and lignin), giving rise to different platform in biorefineries for the production of a wide range of chemicals, which can be obtained after fractionation and depolymerization through thermochemical and enzymatic treatments [1,2].

Focusing on the hemicellulose, this fraction is a biopolymer usually formed by C5 sugars, mainly D-xylose and D-arabinose [3]. This biopolymer can be depolymerized in their respective monosaccharides by hydrolytic processes, which, in turn, can be subsequent dehydrated, obtaining furfural (FUR) as product [4]. FUR is a molecule that has shown great interest, being considered the second most produced molecule in the sugar platform, after bioethanol [5]. The interest of FUR is attributed to its chemical structure (an aldehyde group and a furanic ring with α,β-unsaturation with respect to the aldehyde group), which provides it a high reactivity, leading to a broad spectrum of chemicals through several reactions [6,7]. To date, most of FUR is used to produce furfuryl alcohol (FOL) via hydrogenation [8]. due to its interest in the field of resins [9]. This reaction is industrially carried out using copper chromite as a catalyst [10,11]. However, the search for more environmentally friendly catalysts has led to the development of Cr-free catalysts. In the last decade, a wide variety of studies have been carried out with Cu, Ni, Pd or Pt catalysts, obtaining FOL as product, but also other chemicals, such as 2-methylfuran, 2-methyltetrahydrofuran, furan, tetrahydrofuran or alkanes, among others [12–15].

* Corresponding author at: Departamento de Química Inorgánica, Cristalografía y Mineralogía, Facultad de Ciencias, Universidad de Málaga, Campus de Teatinos, Málaga 29071, Spain.
E-mail address: jacecilia@uma.es (J.A. Cecilia).

https://doi.org/10.1016/j.cattod.2024.115146
Received 4 April 2024; Received in revised form 9 November 2024; Accepted 22 November 2024
Available online 28 November 2024

An alternative to the use of metal-based catalysts for the reduction of FUR into FOL is the use of Lewis acid catalysts [16–18]. This process takes place through a hydrogen catalytic transfer from a secondary alcohol, which acts as sacrificing alcohol, to an aldehyde or ketone via a six membered intermediate [19,20]. This reaction was initially performed in the presence of Al- or Zr-alkoxides [21,22], while Al_2O_3- and ZrO_2-based catalysts have been used more recently [23–27], although other authors have also selected these materials as supports for oxidation reactions of FUR [28,29]. In the same way, other studies have reported that the presence of basic sites can also promote this hydrogen transfer, obtaining FOL as product [30–32]. These studies have gone further, since they can proceed through consecutive reactions in one-pot processes, obtaining other valuable products [33–35]. To this end, several studies have demonstrated the need for the coexistence of Brønsted and Lewis acid sites [33]. The first studies in one-pot processes were carried out using zeolites, where generally the Al species were extracted from the zeolite framework to incorporate Sn, Ti, Hf and mainly Zr species [36–42].

One of the main challenges to achieve good conversions and yields in the one-pot process of FUR to obtain valuable products is the dispersion of the active phase in a porous material. In this sense, several studies have proposed the use of hierarchical materials, such as porous silicas, zeolites or metal-organic frameworks (MOFs) [36–52], which make the process more expensive compared to materials abundant in nature, such as clay minerals [53,54], although with poorer textural properties. In this sense, both biochar and activated carbon can be obtained from very abundant and low-cost sources, in such a way that it is possible to obtain sustainable and cheap porous materials [55]. In this context, agricultural waste is a low-cost source with great potential to provide porous materials under thermal treatment in a non-oxidizing medium to avoid its combustion and to obtain biochars with excellent microporosity. The textural properties of these biochars can be improved with the addition of chemical activators, such as $ZnCl_2$, $FeCl_3$, KOH or H_3PO_4, which promotes condensation, dehydration, or polymerization reactions, giving rise to activated carbon with a wider pore diameter after pyrolysis [56–58].

In the present study, olive stone wastes have been selected as starting material to obtain a carbonaceous material with high porosity. In order to improve the textural properties of the porous carbon, H_3PO_4 has been used as activating agent. This acid exerts two functions. On the one hand, the porosity of the carbonaceous material is improved, and, on the other hand, phosphate groups provide Brønsted acid sites. Then, the Lewis acid sites, necessary for the one-pot process, were incorporated by the addition of Zr species to the activated carbon with phosphoric groups, by impregnation at incipient wetness, and subsequent thermal treatment in an inert atmosphere. In this way, a catalyst with both types of acid sites can be obtained, with great potential for one-pot processes for transforming FUR in valuable chemicals. Finally, it should be noted that both olive stones and furfural are included in the sugar platform, within the framework of biorefineries, so this work can fit within the circular economy concept.

2. Materials and methods

2.1. Synthesis of the catalysts

The activated carbons were synthesized through the chemical activation of agricultural waste (olive stones) provided by Sociedad Cooperativa Andaluza Olivarera y Frutera San Isidro in Periana (Malaga, Spain). Ten grams of this waste were impregnated with 23.5 g of 85 % (w/w) H_3PO_4, to reach a weight ratio of H_3PO_4 to olive stone of 2. The impregnated sample was then activated in a tubular furnace at 800 °C (Carbolite CTF 12/100/900, Thermo Fisher Scientific) under a nitrogen flow of 150 cm^3 STP/min, with a heating rate of 10 °C/min. This activation temperature was maintained for 2 hours. Following activation, the carbonized sample was washed with deionized water at 60 °C until a constant pH was achieved. Finally, the samples were ground and sieved to obtain a particle size range of 100–300 μm.

For catalyst preparation, zirconium was loaded onto the activated carbon, used ad support, using incipient wetness impregnation methodology with a zirconium nitrate ($ZrO(NO_3)_2$) aqueous solution. For this step, 2 g of activated carbon were impregnated with the zirconium salt to incorporate between 0.18 and 0.33 g of ZrO_2, resulting in a final zirconium oxide weight ranging from 5 % to 10 %. The impregnated samples were dried overnight at 120 °C and subsequently calcined at 250 °C in an air atmosphere for 2 hours. The samples were named as ACP-Zr-X, where X denotes the weight percentage of ZrO_2 content.

2.2. Characterization techniques

The textural properties of the ACP-Zr catalysts were assessed through N_2 adsorption-desorption isotherms at −196 ºC and CO_2 adsorption-desorption isotherms at 0 ºC. The crystallinity and phase structure were analyzed using X-ray diffraction (XRD) and Raman spectroscopy. The sample morphology was examined by Transmission Electron Microscopy (TEM). Surface chemical composition of the ACP-Zr catalysts was characterized by X-ray photoelectron spectroscopy (XPS). Acidity measurements were performed via temperature-programmed desorption of pyridine and 2,6-dimethylpyridine. The carbon content of the catalysts, both before and after the reaction, was determined through elemental analysis. Further details regarding each technique can be found in the Supplementary Information.

2.3. Catalytic tests

Catalytic studies for the one-pot transformation of furfural (FUR) into valuable products were carried out in glass pressure reactors with threaded bushings (Ace, 15 mL). In each experiment, 100 mg of catalyst was mixed with 0.1 mmol of FUR and 5 mL of i-propanol, maintaining a 50:1 molar ratio of i-propanol to FUR. Before starting the reaction, the glass reactors were purged with helium for 15 seconds. The reactions were conducted under constant stirring (400 rpm) at temperatures between 110 and 170 ºC for up to 24 hours. The reactors were immersed in an aluminum block for heating, with the temperature controlled via a thermocouple placed directly against the block. Once the reaction was completed, the glass reactors were removed from the block and cooled in water until they reached room temperature. Finally, an aliquot of the reaction medium was then taken, microfiltered, and analyzed by gas chromatography (GC).

For the reuse tests, once the reaction concludes, the reactor is allowed to cool, and an aliquot of the reaction solution is extracted by decantation and microfiltered for analysis via gas chromatography (GC). The catalyst is then filtered and washed with the reaction solvent (i-propanol). Subsequently, the catalyst is dried before proceeding with the next catalytic cycle. In the final cycle, the catalyst is dried and subjected to thermal treatment in a tubular furnace under a nitrogen flow of 60 mL/min, heating from room temperature to 500 ºC, and maintaining this temperature for 2 hours.

All aliquots were analyzed by gas chromatography equipped with a flame ionization detector (FID) and a CP-Wax 52 CB capillary column. The conversion of furfural (FUR) and the product yield were determined using the following calculations:

$$\text{Conversion}(\%) = \frac{\text{mol of furfural converted}}{\text{mol of furfural fed}} \times 100$$

$$\text{Yield}(\%) = \frac{\text{mol of product}}{\text{mol of furfural fed}} \times 100$$

3. Characterization of the catalysts

The determination of the textural properties of the ACP-Zr catalysts

Table 1
Textural properties estimated from N_2 adsorption-desorption isotherms at −196 ºC and CO_2 adsorption at 0 ºC for the ACP-Zr catalysts before and after the catalytic process. Experimental conditions: 170 ºC, 24 h, IpOH/FUR molar ratio of 50, 0.1 g catalyst, FUR/catalyst weight ratio of 1.

Sample	N_2					CO_2	
	S_{BET} (m^2/g)	A_t (m^2/g)	V_t (cm^3/g)	V_{meso} (cm^3/g)	V_{total} (cm^3/g)	A_{DR} (m^2/g)	V_{DR} (cm^3/g)
ACP-Zr−5	1316	505	0.422	0.868	1.290	401	0.161
ACP-Zr−7.5	1249	404	0.435	0.687	1.122	404	0.162
ACP-Zr−10	1196	342	0.428	0.526	0.954	395	0.158
ACP-Zr−5-u	376	186	0.085	0.260	0.345	176	0.081
ACP-Zr−7.5-u	233	36	0.012	0.314	0.326	142	0.066
ACP-Zr−10-u	167	48	0.018	0.175	0.193	164	0.018

was carried from N_2 adsorption-desorption isotherms at −196 ºC (Table 1 and Supplementary Material, Figure S1) and CO_2 adsorption at 0 ºC (Table 1).

The N_2 adsorption-desorption isotherms of ACP-Zr catalysts (Supplementary Material, Figure S1A) can be adjusted between Types I and IV [59], where the high N_2 adsorption at low relative pressure would suggest the existence of microporosity, while the linearity at relative pressure between 0.05 and 0.40 reveals mesoporosity. Regarding the hysteresis loops, all ACP-Zr catalysts exhibit Type H4 [59], which is typical of micro-mesoporous materials, as zeolites or activated carbons. These data agree well with those reported in the literature, since a chemical activation for the preparation of activated carbons promotes the formation of microporosity. However, the addition of activating agents increases the pore width, also favoring a greater microporosity [57]. On the other hand, the isotherms also show how an increase in the Zr content causes a progressive decrease in the amount of adsorbed N_2.

The mesoporosity was determined from the BET equation (Table 1). These data confirm that APC-Zr catalysts display a high surface area with a high microporosity. The pore volume values confirm the coexistence of micro- and mesoporosity. In all cases, the incorporation of Zr species causes a slight worsening of the textural properties, probably due to the Zr species could be deposited on the surface of the ACP causing a partial blockage of the micropores. However, all the catalysts display a high surface area and pore volume, so the Zr content should hardly affect their textural properties.

From the surface data, it can be established that the values of the textural properties hardly decline after the incorporation of Zr species, which are deposited on the external surface of the ACP due to the particle size of these Zr species must be larger than the micropores of the activated carbon. This fact should cause a partial blockage of the micropore entrance such that small molecules such as N_2 or CO_2 can access the narrow pores. However, the entry of larger molecules, such as reactants and/or products, must be more difficult. Therefore, blocking the micropore entrance should render the narrow pores useless.

Considering that N_2 molecules cannot access the narrow micropores, CO_2 adsorption isotherms at 0 ºC were performed, since they can provide interesting information about microporosity (Supplementary Material, Figure S1B). CO_2 molecules can enter more easily into those micropores, due to its higher quadrupolar moment in comparison to N_2. The data reported in Table 1 confirm that the incorporation of Zr species hardly affects microporosity, so Zr species only seem to block slightly the mesoporosity.

The crystallinity of the ACP-Zr catalysts was evaluated by X-ray diffraction (XRD) (Supplementary Material, Figure S2). In all cases, two broad diffraction peaks located at 2θ (º) of 23.8 and 43.7 were observed, corresponding to the typical signals of a graphitic carbon [60]. The width of these diffraction peaks suggests that all catalysts display a low crystallinity. On the other hand, the absence of other diffraction peaks would rule out the segregation of P and/or Zr species.

The determination of the morphology for the ACP-Zr catalysts was performed by Transmission Electron Microscopy (TEM) (Fig. 1 and Supplementary Material, Figure S3). All catalysts display an anisotropic structure, where the porosity is hardly observed. This can be attributed to the high microposity of the activated carbons, as inferred from their textural properties (Table 1 and Supplementary Material, Figure S1). A study of the ACP-Zr catalysts by EDX mapping microanalysis shows how the P species are agglomerated on the surface of the carbonaceous material. Likewise, these studies also suggest that Zr species subsequently incorporated tend to interact with P species.

The Raman spectra show the presence of two bands at 1335 and 1590 cm^{-1}, which are the typical D band of the $A_{1\,g}$ mode in-plane breathing vibration type and the G band associated to the $E_{2\,g}$ in-plane vibration mode of the carbons, respectively (Supplementary Material, Figure S4) [61]. The ratio between both bands (I_D/I_G) can provide interesting information about the structure of the carbonaceous material. In this sense, an increase in the I_D/I_G ratio suggests the formation of a higher proportion of sp^2-hybridization, which is directly related to the formation of a graphitic materials. In all cases, the Raman spectra present a similar I_D/I_G ratio, because the pyrolytic treatment was carried out at the same temperature (800 ºC). On the other hand, the I_D/I_G ratio is in the range of previous studies reported in the literature, where activated carbons were synthesized at different pyrolysis temperatures [62,63]. In these studies, the intensity of the I_D band increases with the temperature, which implies the formation of a graphitic material [61]. The obtained data agree with the XRD patterns, where a lower crystallinity was observed (Supplementary Material, Figure S2). Other bands with lower intensity have also been observed at higher Raman shift values. Thus, the band located about 2685 cm^{-1} is attributed to the 2D graphite layer stacking, which is related to the crystallinity of the graphitic material [64], while the band located at 2910 cm^{-1}, assigned to D+D', is associated with disordered carbon [65].

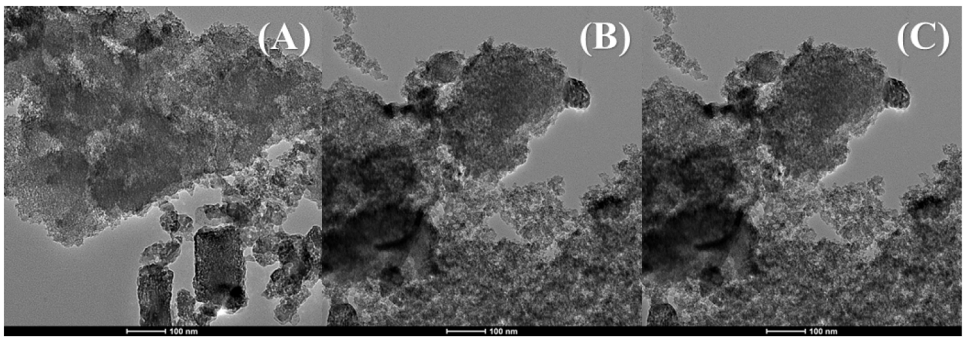

Fig. 1. TEM micrographs for ACP-Zr-5 (A), ACP-Zr-7.5 (B) and APC-Zr-10 (C).

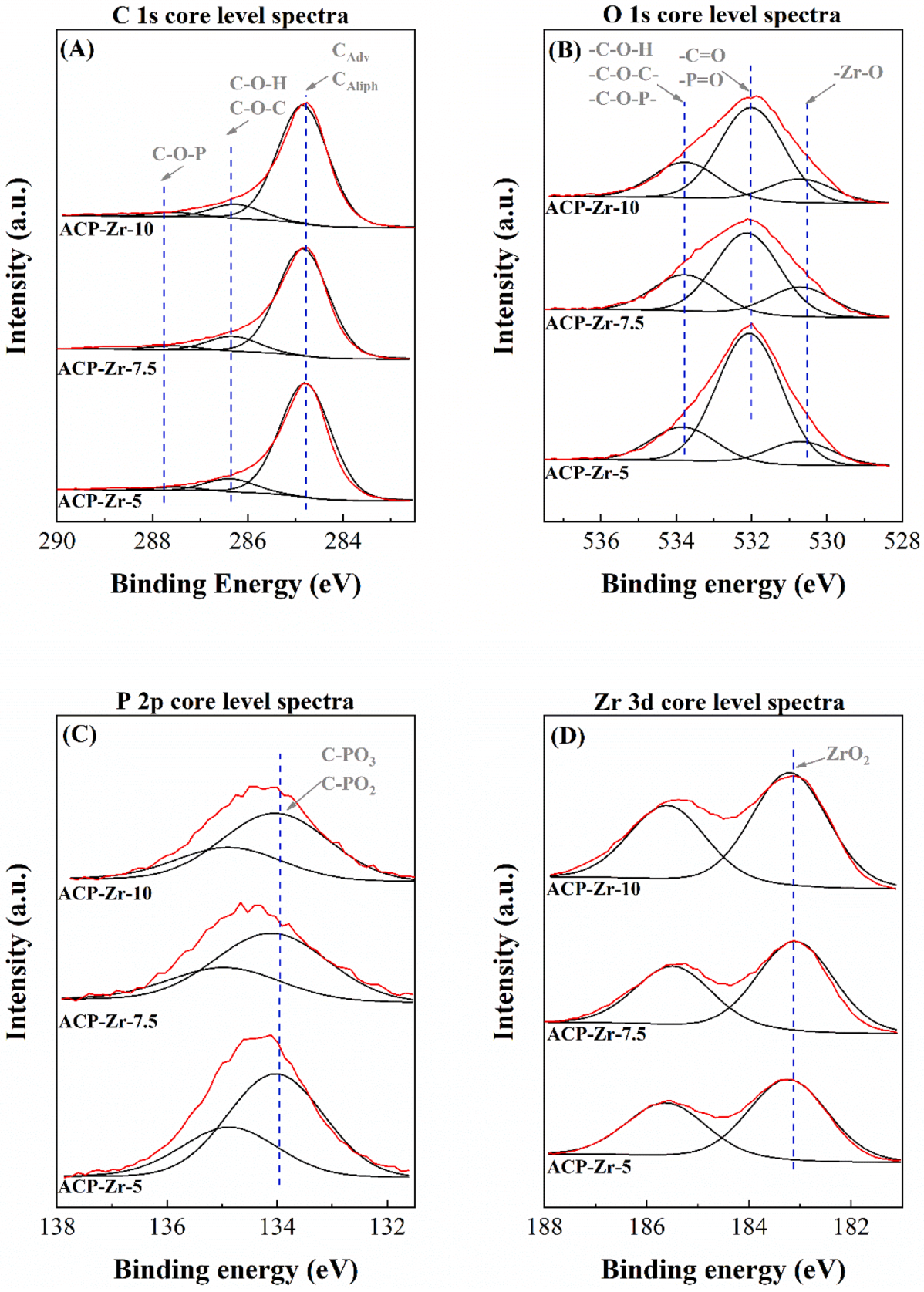

Fig. 2. C 1 s (A), O 1 s (B), P 2p (C), Zr 3d (D) core level spectra of ACP-Zr catalysts.

Table 2
Determination of the atomic concentrations of the ACP-Zr catalysts before and after the catalytic pocess. Experimental conditions: 170 ºC, 24 h, IpOH/FUR molar ratio of 50, 0.1 g catalyst, FUR/catalyst weight ratio of 1.

Sample	Atomic concentration (%)				Molar ratio
	C 1 s	O 1 s	P 2p	Zr 3d	P/Zr
ACP-Zr−5	71.99	21.59	2.97	3.44	0.86
ACP-Zr−7.5	72.92	20.20	2.60	4.28	0.61
ACP-Zr−10	71.89	20.14	2.31	5.66	0.41
ACP-Zr−5-u	81.71	15.59	1.44	1.26	0.87
ACP-Zr−7.5-u	78.45	18.33	1.25	1.97	0.63
ACP-Zr−10-u	78.43	18.09	1.08	2.40	0.45

Table 3
Acidity values determined from pyridine and 2,6-dimethylpyridine thermo-desorption for the ACP-Zr catalysts.

Sample	Pyr-TPD (mmol/g)	2,6-DMPyr-TPD (mmol/g)	Difference (mmol/g)	Brönsted (%)	Lewis (%)
ACP-Zr−5	0.972	0.456	0.516	46.91	53.09
ACP-Zr−7.5	0.912	0.363	0.550	39.75	60.25
ACP-Zr−10	0.909	0.228	0.681	25.05	74.95

The analysis of the surface chemical composition of the ACP-Zr catalysts was carried out by X-ray photoelectron spectroscopy (XPS) (Fig. 2 and Table 2). This analysis confirms that the catalysts are mainly carbonaceous with an atomic concentration of carbon ranging¡ between 71.99 % and 72.92 %. In all cases, the C 1 s core level spectra display three contributions (Fig. 2A): a main contribution at 284.8 eV, which is assigned to both the adventitious carbon and aliphatic carbon species, while the smaller contributions at 286.3 and 287.3 eV reveal to existence of C-O-H/C-O-C and C-O-P bonds, respectively [58,66].

The atomic concentrations of oxygen are in the range of 20.14–21.59 %. In all cases, three contributions are also observed (Fig. 2B). The main contribution appears about 531.9 eV, associated with -C═O, -P═O groups. The smaller contributions, at 533.6 eV and 530.7 eV, are assigned to -C-O-H/-C-O-C-/-C-O-P- and Zr-O groups, respectively [58,67].

Regarding the P species, its surface content is 2.31–2.97 %. In all cases, a single contribution is observed (the smaller contribution is assigned to their respective doublet) (Fig. 2C), which is attributed to C-PO_3 and C-PO_2 groups [67]. Finally, the analysis of the Zr species provides a surface atomic concentration between 3.44 % and 5.66 %. All catalysts display a single contribution in the $3d_{5/2}$ core level spectra (Fig. 2D), which is attributed to ZrO_2 [68]. It is striking how the P 2p band intensity decreases by increasing the Zr content, which would confirm a preferential deposition of the Zr species on P species, as was suggested by TEM (Fig. 1). In fact, P/Zr molar ratio decreases for the catalysts with higher Zr loadings.

The determination of the Lewis and Brønsted acidity data, which may be involved in the one-pot process to convert FUR into valuable products, was carried out from thermo-desorption studies of pyridine and 2,6-dimethylpyridine. It is well known that pyridine can be adsorbed on both types of acid sites [69], while 2,6-dimethylpyridine is specifically adsorbed onto Brønsted ones [70]. The data compiled in Table 3 point out that the amount of adsorbed pyridine is similar for all catalysts (0.909–0.972 mmol/g). The thermo-desorption data of 2, 6-dimethylpyridine suggest that the incorporation of Zr species causes a decrease in the amount of Brønsted acid sites, from 0.456 mmol/g for ACP-Zr-5 0.228 mmol/g for ACP-Zr-10 catalyst. This could be explained by that concluded from other characterization techniques, since it seems that Zr species are preferably found interacting with phosphate groups, as deduced from TEM (Fig. 1) and XPS (Fig. 2 and Table 2) data. This leads to slight differences in the textural properties of the ACP-Zr catalysts (Table 1), since the progressive incorporation of Zr species provokes a decrease in the S_{BET} and pore volume values. The difference between pyridine and 2,6-dimethylpyridine thermo-desorption values can provide the amount of Lewis acid sites (Table 3), which rises from 0.516 to 0.681 mmol/g when the Zr content increases. From these data, it can be concluded that the incorporation of Zr species causes a decrease in the Brønsted acidity, thus replacing the surface Brønsted acid sites by Lewis ones. This is due to the interaction of P-OH groups (Brønsted acid sites) with Zr species (Lewis acid sites)-

4. Catalytic activity

After the physico-chemical characterization of ACP-Zr catalysts, they were tested in the FUR valorization into valuable products in one-pot processes (Scheme 1), using the experimental conditions optimized in previous studies [24,32,48,68].

In the first study, catalysts were assayed at 110 ºC (Fig. 3). The catalytic results show how the FUR conversion increases with the reaction time, and all ACP-Zr catalysts reach full conversion after 24 h; however, the catalytic behavior differs at intermediate reaction times (Fig. 3A). Thus, the catalyst with the highest Zr content attains higher conversion values at shorter reaction times.

Regarding the products, furfuryl alcohol (FOL) and isopropyl furfuryl ether (IpFE) were detected at shorter reaction times. The formation of FOL is promoted when the Zr content increases, achieving the highest yield (35 %) with ACP-Zr-10, after 90 min at 110 ºC (Fig. 3B). The use of longer reaction times causes a progressive decrease in the FOL yield, which is accompanied by a progressive increase in the IpFE yield (Fig. 3C). It is striking that the catalyst with the highest IpFE yield was that catalyst with the lowest Zr content, attaining a maximum value of 57 % for ACP-Zr-5 after 24 h at 110 ºC. Previous studies have revealed that the reduction of FUR to FOL takes place on basic or Lewis acid sites, using an alcohol as H donor, through a six-membered intermediate [33, 48]. In this study, the Lewis acid sites are provided by Zr species. So the catalyst with the highest amount of Lewis acid sites, i.e. ACP-Zr-10 (Table 3), was that one with the highest FOL yield at shorter reaction time, confirming the role of the Lewis acidity in the first stage of the one-pot process [33]. Regarding the etherification of FOL with isopropanol to obtain IpFE, this can occur with the participation of Lewis or Brønsted acid sites. In this sense, the Lewis acid sites are provided by the presence of Zr species [33,48], while the Brønsted acid sites are associated with phosphate groups [33]. Thus, the catalyst with the highest amount of Brønsted acid sites (ACP-Zr-5) reaches the biggest yield in the etherification product, although the rate of this process seems to be slower than the formation of FOL, at least at 110 ºC. Thus, an IpFE yield of 56 % is reached for the ACP-Zr-5 catalyst after 24 h at this temperature.

In the case of ACP-Zr catalysts with higher Zr contents, a large proportion of IpFe is transformed into isopropyl levulinate (IpL) (Fig. 3D), resulting from the opening of the furan ring. This reaction is promoted by the existence of Brønsted sites associated with phosphate groups [33]. However, those catalysts with a lower Brønsted acidity display a greater activity, reaching a maximum IpL yield of 24 % for ACP-Zr-10, after 24 h at 110 ºC. Despite the decay of the Brønsted acidity, due to the interaction of phosphate groups with Zr species, in a subsequent step, this smaller proportion of Brønsted acid sites seems to be enough for the opening of the furan ring and the formation of IpL.

Finally, undetected products must also be considered, whose formation is favored with the reaction time, due to FUR and FOL are prone to undergo polymerization reactions, giving rise to humins and other polymeric species, as inferred from the dark color of the reaction media [48]. Thus, the data compiled in Fig. 3E show that the amount of non-detected products increases for those catalysts with a higher catalytic activity, with values between 15 % and 33 %, after 24 h at 110 ºC.

On the other hand, it has been previously reported that one-pot processes of FUR to obtain valuable products usually require high reaction temperatures [42,46,48]. Therefore, the reaction was also carried

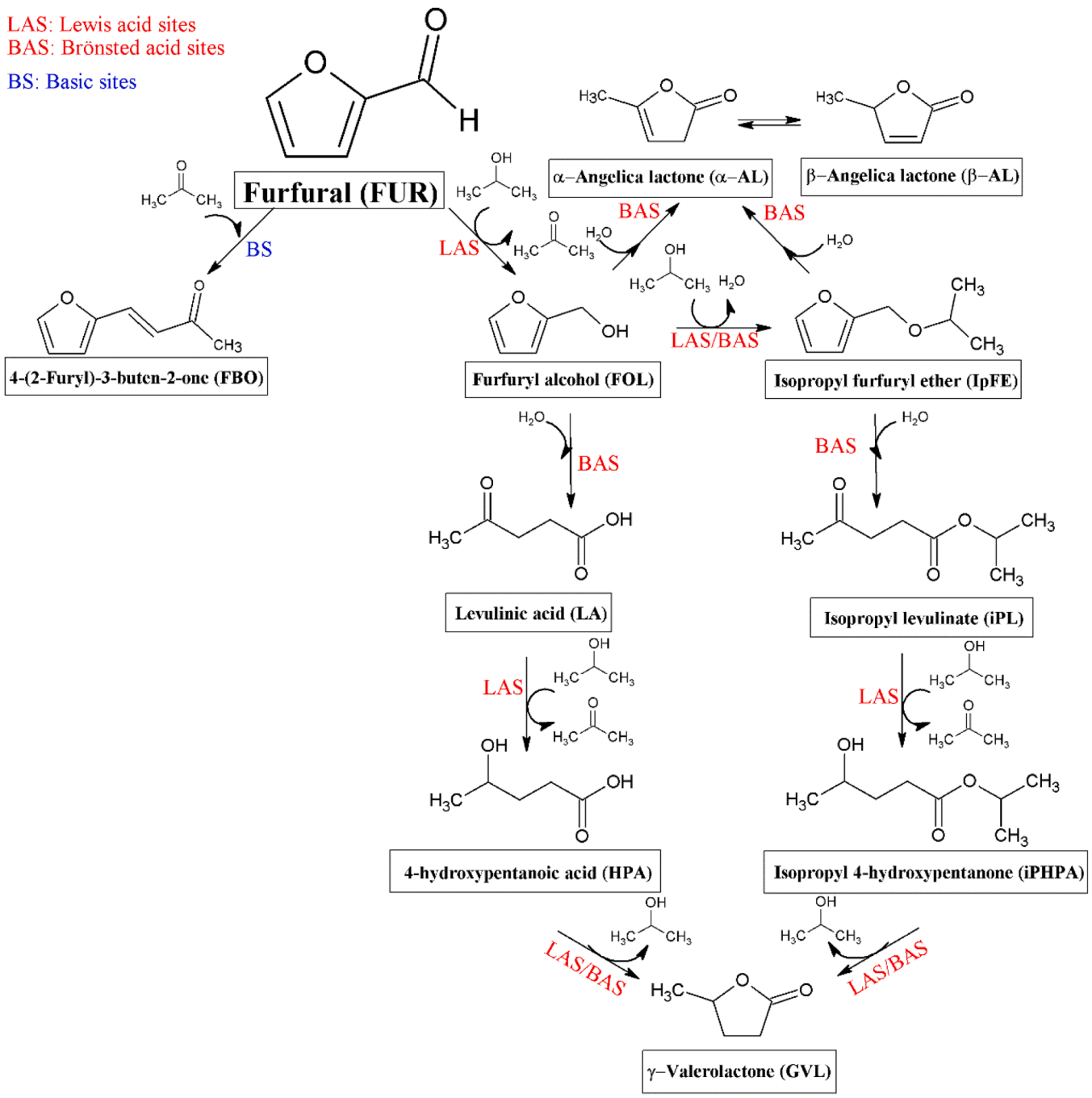

Scheme 1. Route of the one-pot process of FUR into valuable products.

out at 170 °C (Fig. 4). Full furfural conversion is obtained after only 45 min for all ACP-Zr catalysts (Fig. 4A), although the product patterns differ.

In all cases, FOL is only obtained at short reaction times, showing a similar yield profile, since a maximum value close to 20 % is reached after 30 min due to the presence of Lewis acid sites (Fig. 4B). Then, FOL disappears at longer reaction time to form other products. The IpFE yield follows the same trend for all catalysts, since the highest yield (about 50 %) is obtained after 1 h. These values are higher than those observed at 110 °C, suggesting that the etherification reaction is promoted at higher reaction temperature. In the same way, Fig. 4C also shows how the decrease in the IpFE yield along the time is less pronounced than that reported for FOL (Fig. 4B), suggesting that IpFE is less reactive than FOL even at higher temperature.

Once FOL and IpFE decay, the presence of Brønsted acid sites promotes the formation of IpL (Fig. 4D), reaching the maximum yield between 90 min and 6 h. In this case, the IpL yield is directly related to the Zr content, and the catalyst with the lowest Zr loading (ACP-Zr-5) displays the maximum IpE yield, with a value of 35 % after 6 h, which decays until 24 % after 24 hours of reaction at 170 °C. The decrease observed for higher Zr contents could be ascribed to their higher amount of Lewis acid sites, which promote the reduction of the carbonyl group of IpL and its subsequent lactonization to form gamma-valerolactone (GVL), achieving a maximum GVL yield of 36 % after 24 h at 170 °C for ACP-Zr-10 (Fig. 4E). It has been previously demonstrated that the formation of GVL is the limiting step in one-pot processes of FUR, since higher temperature and long reaction time are required for the final lactonization, as was detected for other Zr-based catalysts [38,44].

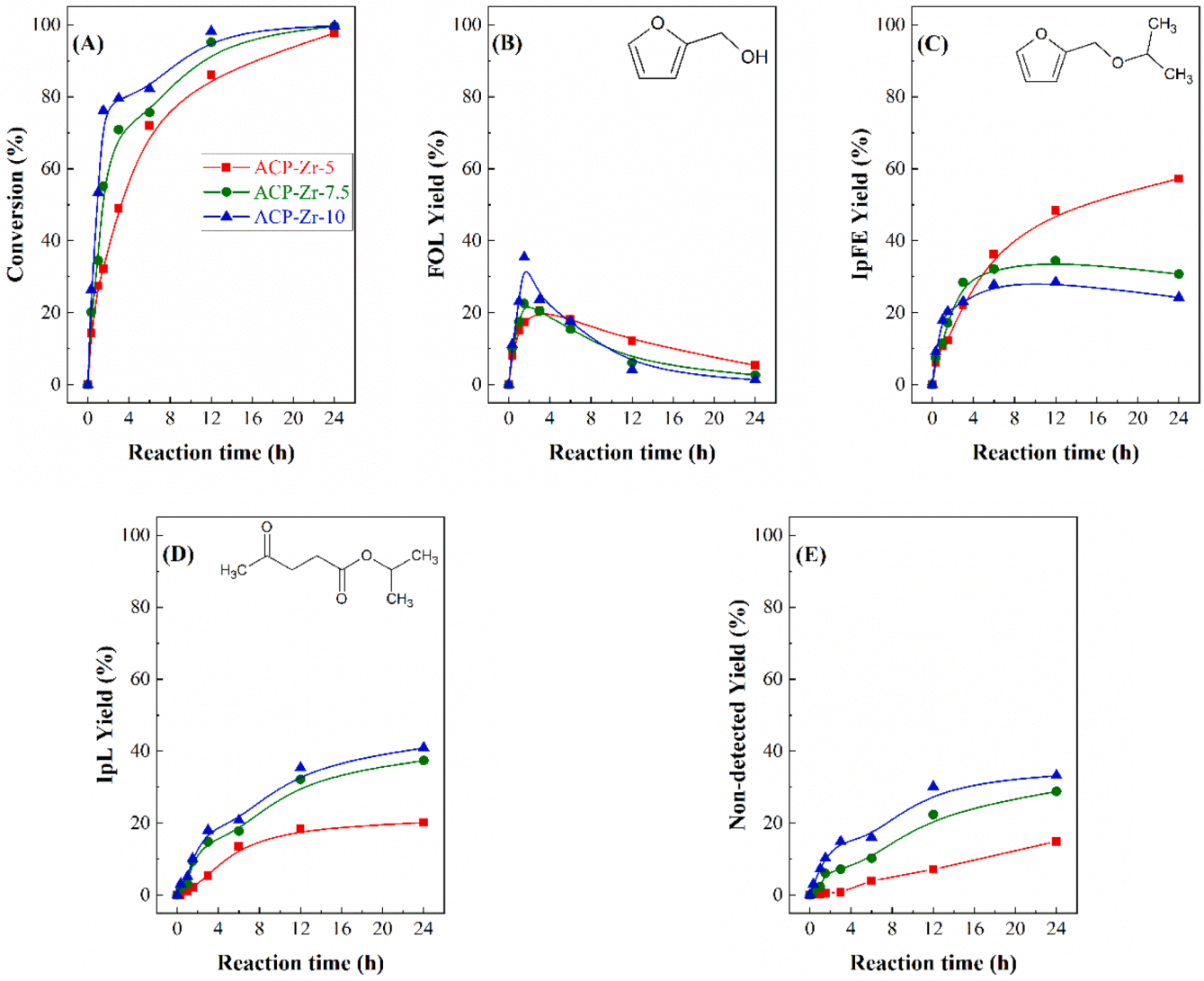

Fig. 3. FUR conversion (A), FOL yield (B), IpFE yield (C), IpL yield (D) and non-detected (E) in the one-pot process of FUR using ACP-Zr catalysts. Experimental conditions: 110 ºC, IpOH/FUR molar ratio of 50, 0.1 g catalyst, FUR/catalyst weight ratio of 1.

Other products, such as angelica lactones (AL) (Figs. 4F) and 4-(2-furyl)-3-buten-2-one (FBO) (Fig. 4G) have been detected, although their yields do not exceed 10 % at any reaction time.

Finally, all catalysts display a high proportion of non-detected products, which is higher than those observed at 110 ºC. The catalytic results indicate that an increase in the Zr content favors the formation of non-detected products, probably due to undesired polymerization reactions of FUR or FOL, which tend to form humins.

The catalytic results (Figs. 3 and 4) show that these catalysts are highly selective towards IpFE at 110 ºC, while the formation of IpL is favored at 170 ºC. Considering that the temperature has a clear influence on the product pattern, the next study was focused on the analysis of the role of the temperature on the catalytic behavior, maintaining a reaction time of 6 h (Fig. 5). Despite ACP-Zr catalysts reach higher FUR conversions when the temperature increases, the selectivity patterns are different. Thus, FOL and IpFE are preferably formed at lower temperature, suggesting that these products are those obtained in the first stages of the one-pot process. As was indicated above, the first step takes place through the participation of Lewis acid sites to form FOL. Then, the etherification to form IpFE occurs on Lewis or Brønsted acid sites. Previous studies have reported that Al-based catalysts, which possess Lewis acid sites, promote the formation of FOL [24]. The presence of Brønsted acid sites seems to favour the etherification of FOL into IpFE, at least at lower temperature and faster than Lewis acid sites [33,44,48]. In this way, FOL levels decrease progressively, while IpFE levels increase with temperature. The increase in the reaction temperature also leads to the formation of other products. Thus, all APC-Zr catalysts exhibit an increase in the IpL yield with the reaction temperature by the presence of phosphate groups, which act as Brønsted acid sites [33]. Finally, GVL requires the coexistence of Lewis acid sites to the reduction of the ketone group in the IpL and Brønsted acid sites for a final lactonization to give rise to GVL. As was indicated previously, this final lactonization reaction requires more severe experimental conditions, being the limiting step in the one-pot process [44]. In addition, other products coming from side-reactions are observed. For example, FBO is detected in minor proportions. This product is obtained by an aldol reaction between the remaining FUR with acetone, which is obtained in the CTH process from the secondary alcohol (i-propanol) in the reduction of FUR into FOL. This reaction can take place by the presence of basic [71] or Lewis acid sites, requiring higher temperature [72]. The increase in the reaction temperature also leads to the formation of non-detected products due to uncontrolled condensation reactions [48,68].

The number of studies where Zr species are dispersed in carbonaceous materials for the valorization of furfural in one-pot is limited [55,

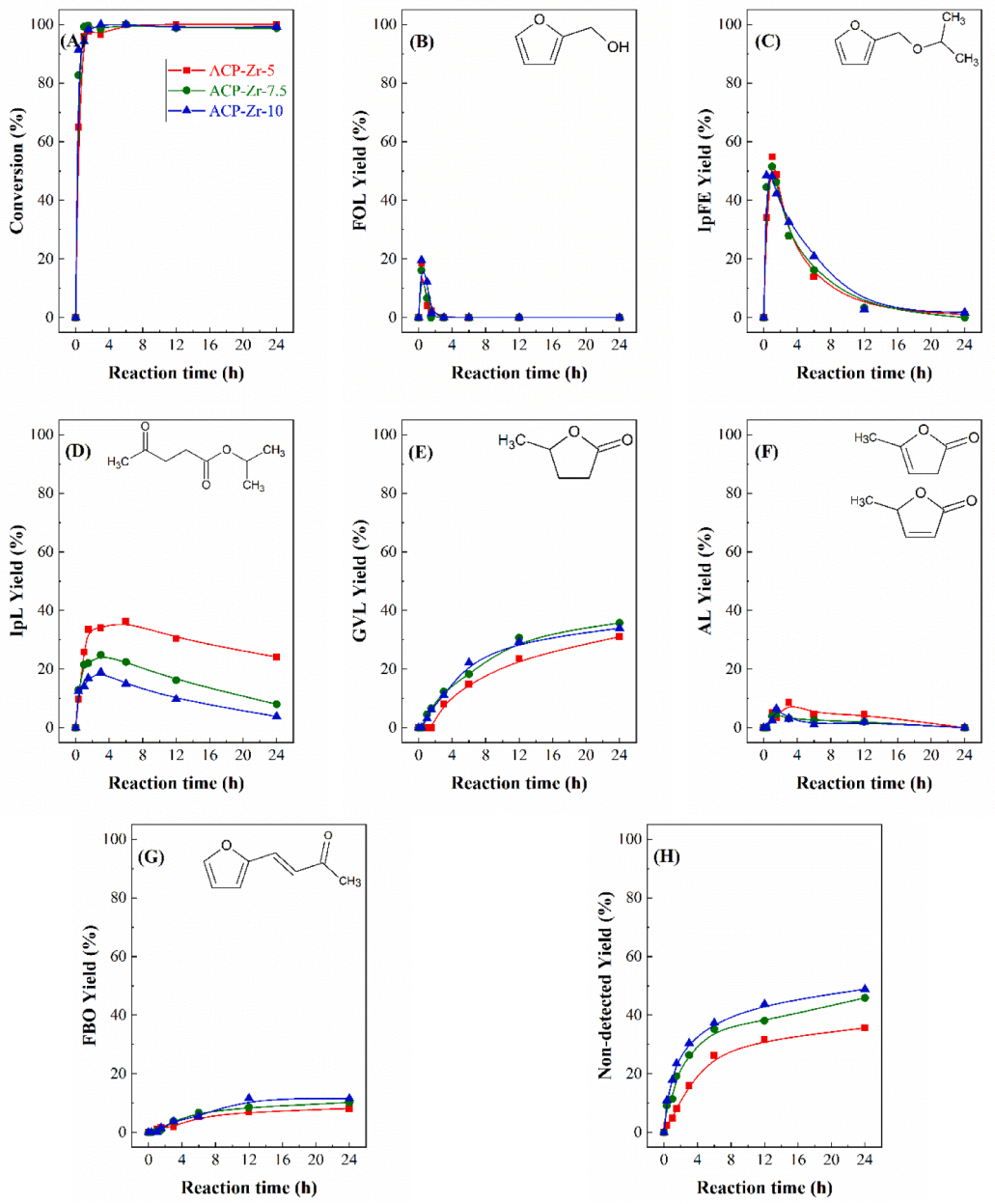

Fig. 4. FUR conversion (A), FOL yield (B), IpFE yield (C), IpL yield (D) GVL yield (E), AL yield (F), FBO yield (G) and non-detected (H) in the one-pot process of FUR using ACP-Zr catalysts. Experimental conditions: 170 ºC, IpOH/FUR molar ratio of 50, 0.1 g catalyst, FUR/catalyst weight ratio of 1.

73]. In a first study, a Zr-graphitic carbon nitride/H-β composite was used as catalyst [55]. Thus, the Brønsted acid sites are provided by the β-zeolite, while the Lewis acid sites are associated with the Zr species, obtaining high yield of GVL, although the experimental conditions are slightly different. In another study, Zr species were incorporated into a carbonaceous material [73]. In this case, the absence of Brønsted acid sites limits the reaction to the formation of FOL. Considering the obtained results and those reported in the literature, it is necessary the coexistence of Lewis and Brønsted acid sites to obtain GVL as product. In the present study, the Brønsted acid sites are provided by the presence of phosphate groups, while the Lewis acid sites are generated by the existence of Zr species in the catalyst.

In order to evaluate the reuse of the ACP-Zr catalysts, the most active catalyst (ACP-Zr-10) was tested during several catalytic cycles at 110 and 170 ºC, for 24 h (Fig. 6). At the lowest temperature, full conversion is attained, obtaining IpL and IpFE as main products after the first cycle. However, this profile is modified when the number of cycles increases, being observed that FUR conversion decreases from 100 % to 64 % after the fourth cycle. In addition, the product patterns are also modified. Thus, IpFE and, mainly, IpL, decrease after each cycle, while FOL increases from 1 % to 15 %. A similar conversion decrease is also observed at 170 ºC (from 100 % to 80 % after the 4th cycle), confirming that this decay is less pronounced than that observed at 110 ºC. Regarding the products, it is noteworthy that the GVL yield decreases notably from 34 % to 2 %. This decrease is accompanied by a rise in FOL, IpFE and IpL after each cycle. From the data obtained for the ACP-Zr-10 after several cycle at 110 and 170 ºC, it can be concluded that the reaction is retained in earlier reaction stages of the one-pot process as the number of cycles increases.

In order to achieve conversion and yield values similar to those obtained after the 1st reaction cycle, the catalysts were thermally treated in a N_2 flow at 500 ºC to remove carbonaceous deposits on the surface. Unfortunately, the values do not achieve the obtained results after the 1st cycle although they are very close. This decrease can be attributed to

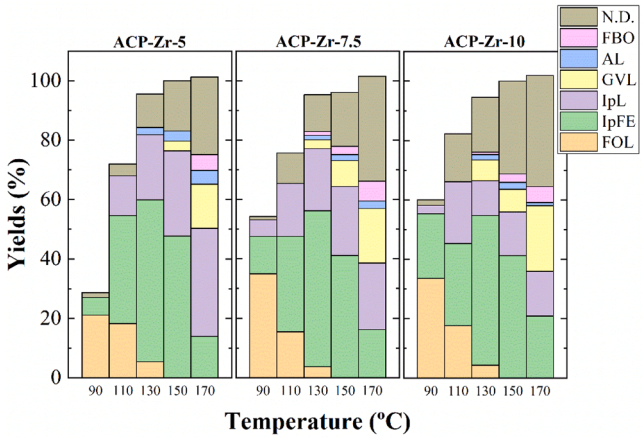

Fig. 5. FOL, IpFE, IpL, GVL, AL, FBO and non-detected yields in the one-pot process of FUR using ACP-Zr catalysts. Experimental conditions: 90–170 ºC, 6 h, IpOH/FUR molar ratio of 50, 0.1 g catalyst, FUR/catalyst weight ratio of 1.

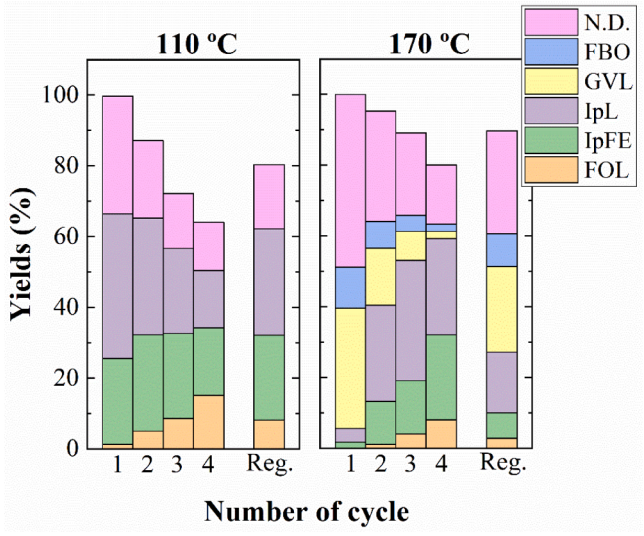

Fig. 6. FOL, IpFE, IpL, GVL, AL, FBO and non-detected yields in the one-pot process of FUR using ACP-Zr-10 for four catalytic cycles. Experimental conditions: 170 ºC, 24 h, IpOH/FUR molar ratio of 50, 0.1 g catalyst, FUR/catalyst weight ratio of 1.

the sintering of the Zr species or a blockage of the active sites, because the carbonaceous deposits can be transformed into layers of activated carbon, which must block the active sites involved in the one-pot reaction.

The variation of the conversion and the yield of the products obtained after several cycles suggests that a modification of the active phase must take place. For this purpose, the textural properties of the ACP-Zr catalysts were studied after the reaction at 24 h at 170 ºC. This analysis (Table 2 and Fig. 7) reveals a worsening of the textural properties, as indicate the decrease in specific surface area and pore volume values, which would imply a decline in the amount of available active sites involved in the one-pot process. This would lead to a progressive drop in the FUR conversion, as well as the modification of the selectivity pattern, obtaining products that appears in earlier stages in the one-pot process, as FOL and IpFE, after several cycles (Fig. 6). On the other hand, the Zr leached should be discarded since the Zr-species in the reaction medium after 24 hours of reaction at 170 ºC is in the range of 0.002–0.004 % (Supplementary Information, Table S1).

The surface composition of the used catalyst was also analyzed by XPS. The data shown in Fig. 8 and Table 2 reveal a slight increase in the C content in all catalysts, while the surface concentrations of O, P and Zr decrease after the reaction at 170 ºC for 24 h. This would suggest the formation of carbonaceous deposits on the catalyst surface due to the polymerization of FUR and FOL, which would cover the available acid sites. This fact is also confirmed by the increase in the contribution ascribed to -C-O-C- and -C-O-H groups in the O 1 s core level spectra. The formation of these carbonaceous deposits is directly related to the decay of the FUR conversion and the modification of the selectivity pattern observed after several cycles (Fig. 6). These data have been confirmed by elemental analysis, since the C-content increases in all catalyst after the reaction at 170 ºC.

Considering that the one-pot process can take place on basic sites as well as Lewis and Brønsted acid sites, additional tests were performed to understand the role of the acid and basic sites in the one-pot process of FUR. For this purpose, catalytic tests were carried out with the addition of an acid molecule (benzoic acid), which would neutralize the basic sites, or the addition of basic molecules (pyridine or 2,6-dimethylpyridine) to neutralize the acid sites [25,74] (Fig. 9). The catalytic data, reported in Fig. 9A, shows how the addition of both types of molecules exerts an adverse effect on the catalytic behavior, mainly at shorter reaction times. Thus, the addition of benzoic acid causes a low decrease in the FUR conversion, although total conversion is attained after 12 h at 170 ºC. However, the addition of basic molecules has a more detrimental effect on the catalytic behavior, since, after the addition of 2,6-dimethylpyridine, a conversion value of 95 % was only reached after 24 h at 170 ºC, while the addition of pyridine only provided a FUR conversion of 30 % under similar experimental conditions (24 h at 170 ºC). However, these molecules mainly affected the product yields (Fig. 9B-H).

The addition of benzoic acid to the reaction medium has a limited effect on the catalytic behavior, since FOL formation is similar to that attained without additives, although the decay of FOL requires longer reaction time. In the same way, the formation of IpFE takes place at longer reaction times, although its decay is also more progressive. In the case of IpL, the addition of benzoic acid favors the formation of this product, since IpL hardly decays after long reaction times. Finally, GVL formation is slightly lowered in the presence of additives. From the conversion and yield data, it can be established that the addition of benzoic acid, which should block the basic sites, hardly has any effect on the catalytic behavior. This means that the basic sites have a low influence on the catalytic behavior.

As indicated previously, the addition of 2,6-dimethylpyridine and mainly pyridine, with similar basicity (pK_b values of 7.3 and 8.8, respectively), has a greater inhibitory effect. In this sense, previous studies have reported that 2,6-dimethylpyridine has potential to block the Brønsted acid sites [69,70]. In this reaction, the main products are FOL, at short reaction time, and IpFE, at longer, so the reaction is retained in earlier stages of the one-pot process. However, the ring opening to form IpL, which requires Brønsted acidity, is not promoted. The addition of pyridine has a more drastic effect on the catalytic performance, since both the Lewis and Brønsted acid sites are blocked [69,70]. This supposes a lower FUR conversion, obtaining a very low FOL yield in comparison to the other tests. Therefore, it can be inferred that the acid sites have a predominant effect in the one-pot process. Amongst them, the blockage of the Brønsted acid sites would stop the reaction in IpFE and FOL, while the conversion is very poor when all acid sites are blocked.

5. Conclusions

Activated carbons have been synthesized by the pyrolysis of olive stones using H_3PO_4 as activating agent. The addition of H_3PO_4 has two objectives. On the one hand, this activating agent increases the pore width of the resulting carbonaceous material. On the other hand, the presence of these phosphate groups affects the pyrolytic treatment and provides Brønsted-type acid sites. Then, the Zr species incorporate Lewis

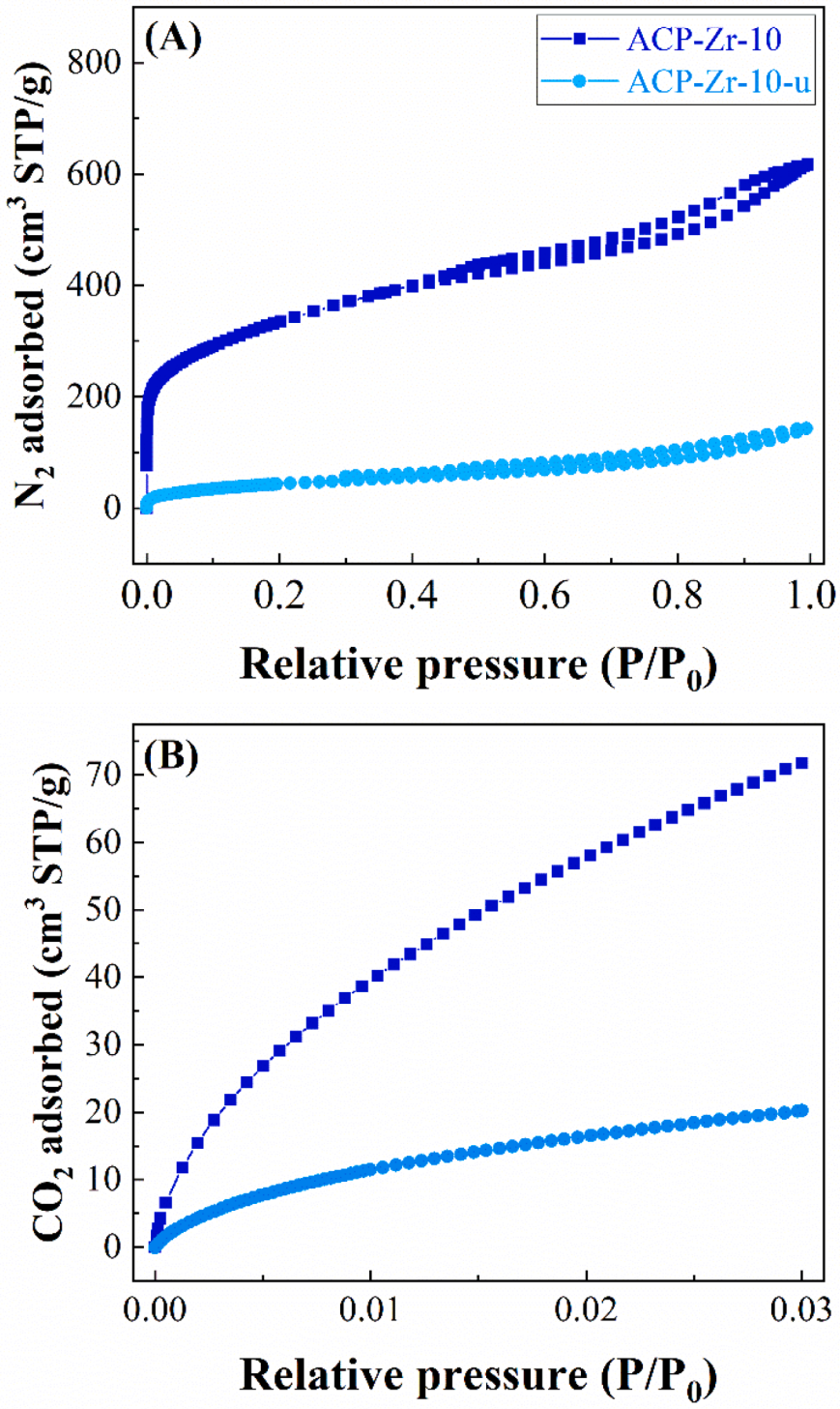

Fig. 7. Comparison of N_2 adsorption-desorption isotherms at −196 °C (A) and CO_2 sorption at 0 °C (B) for the ACP-Zr-10, before and after the catalytic process. Experimental conditions: 170 °C, 24 h, IpOH/FUR molar ratio of 50, 0.1 g catalyst, FUR/catalyst weight ratio of 1.

acidity.

ACP-Zr materials are highly micro- and mesoporous. The P species are slightly agglomerated in the activated carbon and the Zr species, which are added in a subsequent step, are prone to interact preferentially with the phosphate groups.

Considering the coexistence of Lewis and Brønsted acid sites, the ACP-Zr catalysts were tested in the one-pot process of FUR to obtain high value-added chemicals. The catalytic study at low temperature (110 °C) reveals that the catalysts are selective to IpFE, while the use of higher temperature (170 °C) shows IpL and GVL as main products. In all cases, the obtained products are highly interesting, since they can be used as fuel additives or solvents. One of the main disadvantages of this reaction is related to the formation of high levels of humins, which lead to the formation of carbonaceous deposits that block the available active sites. This blockage of the active sites is reflected in the modification of the selectivity patterns obtained after several catalytic cycles, since the reaction is retained in earlier stages in the one-pot of FUR.

In summary, a series of catalysts has been synthesized from a

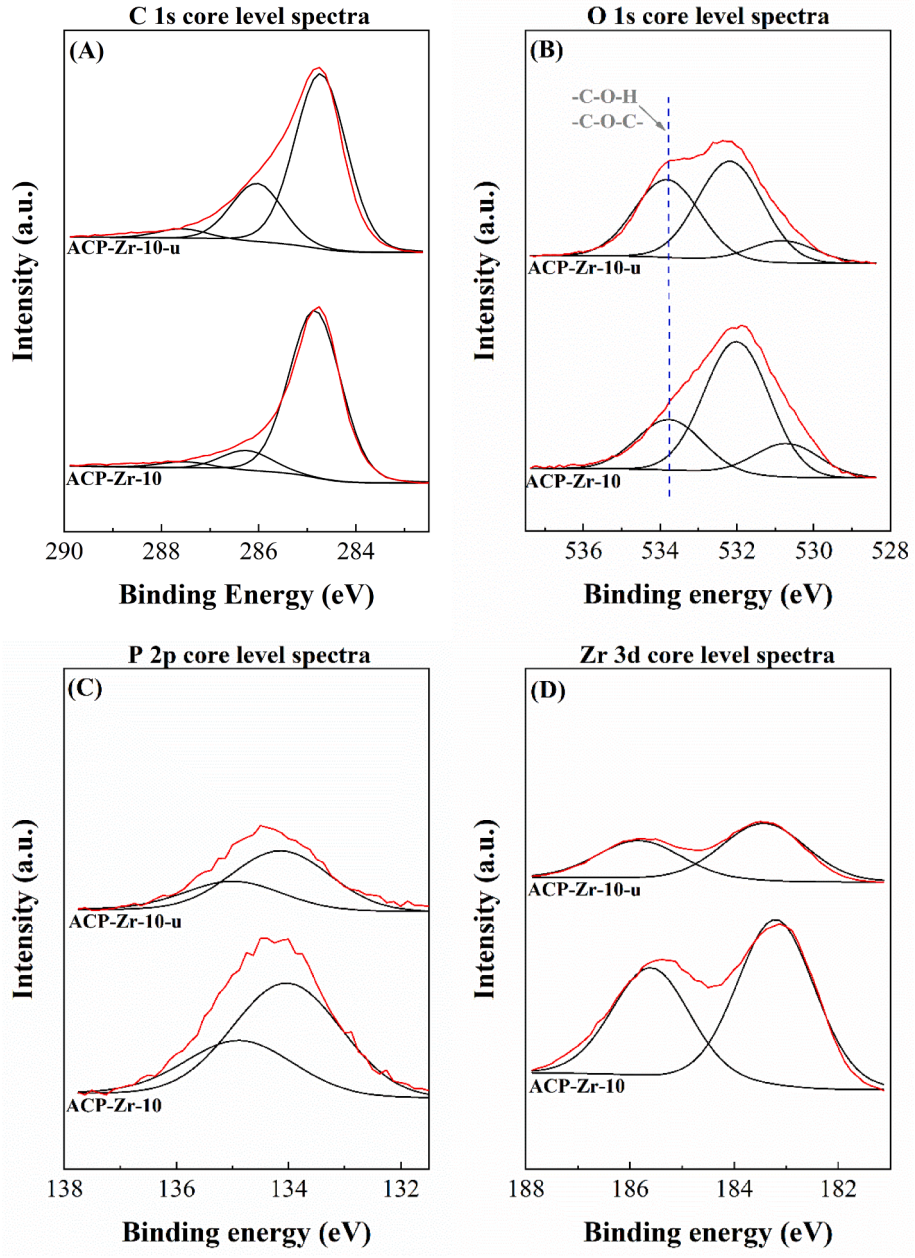

Fig. 8. Comparison of the C 1 s (A), O 1 s (B), P 2p (C) and Zr 3d (D) core level spectra for the ACP-Zr-10, before and after the catalytic process. Experimental conditions: 170 ºC, 24 h, IpOH/FUR molar ratio of 50, 0.1 g catalyst, FUR/catalyst weight ratio of 1.

lignocellulosic waste (olive stones), and used for the valorization of a platform molecule, like FUR, which comes from hemicellulose fraction. In this way, this work can be included within a sustainable and circular economy, since a catalyst is obtained from an inexpensive waste, which is used to obtain high value-added products.

CRediT authorship contribution statement

Tomás Cordero: Writing – review & editing, Validation, Supervision, Resources, Project administration, Funding acquisition, Conceptualization. **Pedro Maireles-Torres:** Writing – original draft, Supervision, Project administration, Funding acquisition, Formal analysis, Data curation. **José Rodríguez-Mirasol:** Validation, Supervision, Resources, Project administration, Funding acquisition. **Juana María Rosas:** Supervision, Methodology, Conceptualization. **Ramón Moreno-Tost:** Validation, Supervision, Project administration, Methodology, Data curation. **Gabriela Rodríguez-Carballo:** Investigation, Formal analysis. **Cristina García-Sancho:** Writing – review & editing, Supervision, Methodology. **Rocío Maderuelo-Solera:** Investigation, Formal analysis. **Francisco José García-Mateos:** Writing – original draft, Investigation, Formal analysis, Data curation. **Juan Antonio Cecilia:** Writing – original draft, Software, Methodology, Investigation, Data curation, Conceptualization.

Declaration of Competing Interest

The authors declare the following financial interests/personal relationships which may be considered as potential competing interests: Juan Antonio Cecilia reports financial support was provided by Spanish Ministry of Science and Innovation and FEDER funds. Juan Antonio Cecilia reports a relationship with University of Malaga that includes: employment. If there are other authors, they declare that they have no

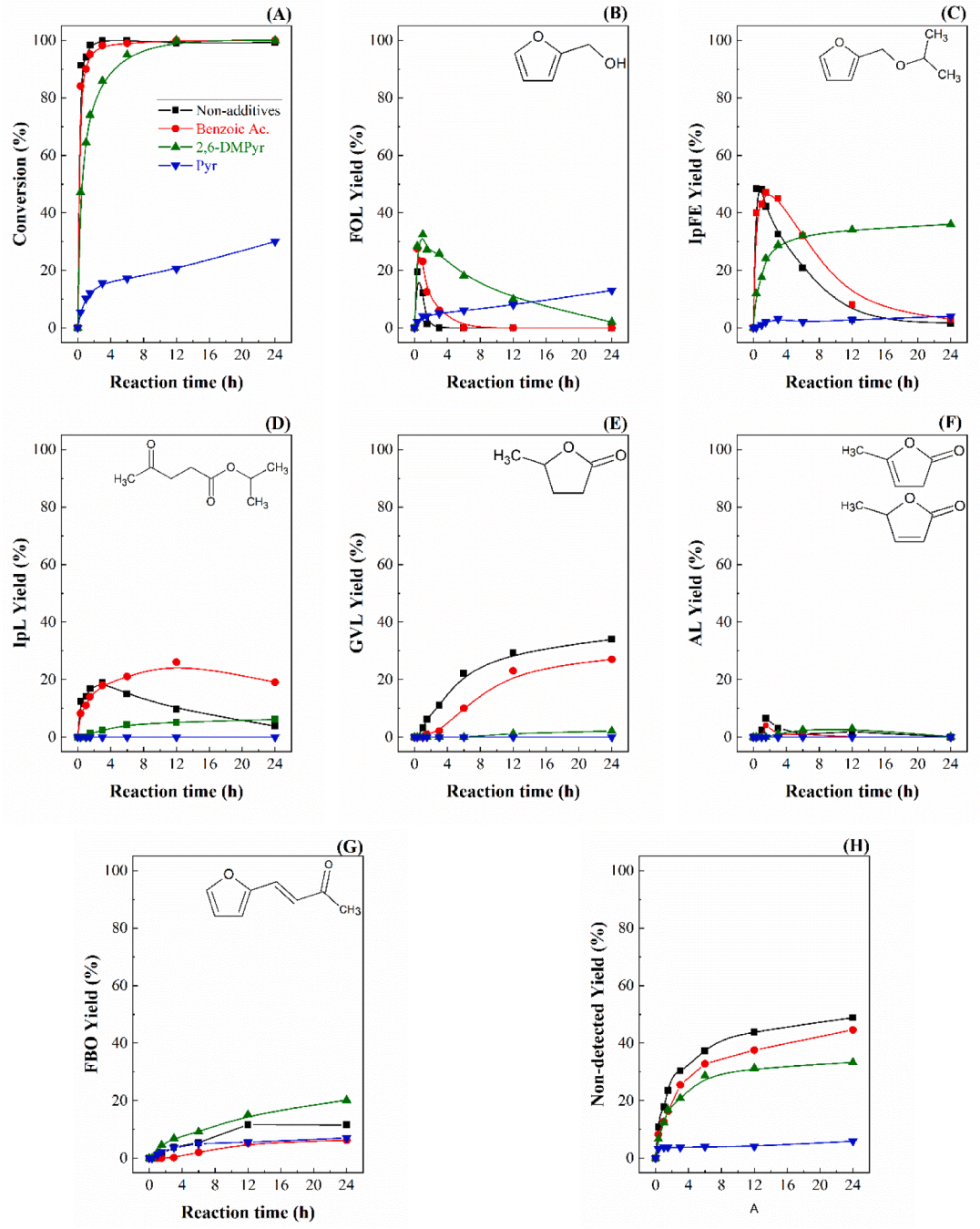

Fig. 9. Effect of the addition of acid (benzoic acid) and basic molecules (pyridine or 2,6-dimethylpyridine). FUR conversion (A), FOL yield (B), IpFE yield (C), IpL yield (D) GVL yield (E), AL yield (F), FBO yield (G) and non-detected (H) in the one-pot process of FUR using ACP-Zr catalysts. Experimental conditions: 170 °C, IpOH/FUR molar ratio of 50, 0.1 g catalyst, FUR/catalyst weight ratio of 1.

known competing financial interests or personal relationships that could have appeared to influence the work reported in this paper.

Acknowledgments

This research was funded by the Spanish Ministry of Science and Innovation (PID2021–122736OB-C42, PID2022–1408440B–I00, TED-2021–131324B–C21), FEDER (European Union) Junta de Andalucia funds (P20–00375, FQM-155-G-FEDER, UMA20-FEDERJA88).

Appendix A. Supporting information

Supplementary data associated with this article can be found in the online version at doi:10.1016/j.cattod.2024.115146.

Data availability

Data will be made available on request.

References

[1] M.V. Rodionova, A.M. Bozieva, S.K. Zharmukhamedov, Y.K. Leong, J.C.W. Lan, A. Veziroglu, T.N. Veziroglu, T. Tomo, J.S. Chang, S.I. Allakhverdiev,

A comprehensive review on lignocellulosic biomass biorefinery for sustainable biofuel production, Int. J. Hydrog. Energy 47 (2022) 1481–1498, https://doi.org/10.1016/j.ijhydene.2021.10.122.
[2] H. Chen, Chemical composition and structure of natural lignocellulose. In: Biotechnology of Lignocellulose, Springer, Dordrecht, 2014, https://doi.org/10.1007/978-94-007-6898-7_2.
[3] T. Yi, H. Zhao, Q. Mo, D. Pan, Y. Liu, L. Huang, H. Xu, B. Hu, H. Song, From cellulose to cellulose nanofibrils - a comprehensive review of the preparation and modification of cellulose nanofibrils, Materials 13 (2020) 5062, https://doi.org/10.3390/ma13225062.
[4] L. Ye, Y. Han, X. Wang, X. Lu, X. Qi, H. Yu, Recent progress in furfural production from hemicellulose and its derivatives: conversion mechanism, catalytic system, solvent selection, Molecul. Catal. 515 (2021) 111899, https://doi.org/10.1016/j.mcat.2021.111899.
[5] W. Adhami, A. Richel, C. Len, A review of recent advances in the production of furfural in batch system, Molecul. Catal. 545 (2023) 113178, https://doi.org/10.1016/j.mcat.2023.113178.
[6] A. Jaswal, P.P. Singh, T. Mondal, Furfural – a versatile, biomass-derived platform chemical for the production of renewable chemicals, Green. Chem. 24 (2022) 510–551, https://doi.org/10.1039/D1GC03278J.
[7] X. Zhang, S. Xu, Q. Li, G. Zhou, H. Xia, Recent advances in the conversion of furfural into bio-chemicals through chemo- and bio-catalysis, RSC Adv. 11 (2021) 27042–27058, https://doi.org/10.1039/D1RA04633K.
[8] D.S.S. Jorqueira, L.F. de Lima, S.F. Moya, L. Vilcocq, D. Richard, M.A. Fraga, R. S. Suppino, Critical review of furfural and furfuryl alcohol production: past, present, and future on heterogeneous catalysis, Appl. Catal. A: Gen. 665 (2023) 119360, https://doi.org/10.1016/j.apcata.2023.119360.
[9] S. Hayashi, A. Narita, T. Wasano, Y. Tachibana, K. Kasuya, Synthesis and cross-linking behavior of biobased polyesters composed of bi(furfuryl alcohol), Eur. Polym. J. 121 (2019) 109333, https://doi.org/10.1016/j.eurpolymj.2019.109333.
[10] R. Rao, A. Dandekar, R.T.K. Baker, M.A. Vannice, Properties of copper chromite catalysts in hydrogenation reactions, J. Catal. 171 (1997) 406–419, https://doi.org/10.1006/jcat.1997.1832.
[11] D. Liu, D. Zemlyanov, T. Wu, R.J. Lobo-Lapidus, J.A. Dumesic, J.T. Miller, C. L. Marshall, Deactivation mechanistic studies of copper chromite catalyst for selective hydrogenation of 2-furfuraldehyde, J. Catal. 299 (2013) 336–345, https://doi.org/10.1016/j.jcat.2012.10.026.
[12] K. Yan, G. Wu, T. Lafleur, C. Jarvis, Production, properties and catalytic hydrogenation of furfural to fuel additives and value-added chemicals, Renew. Sustain. Energy Rev. 38 (2014) 663–676, https://doi.org/10.1016/j.rser.2014.07.003.
[13] Y. Wang, D. Zhao, D. Rodríguez-Padrón, C. Len, Recent advances in catalytic hydrogenation of furfural, Catalysts 9 (2019) 796, https://doi.org/10.3390/catal9100796.
[14] J. Zhang, D. Li, H. Yuan, S. Wang, Y. Chen, Advances on the catalytic hydrogenation of biomass-derived furfural and 5-hydroxymethylfurfural, J. Fuel Chem. Technol. 49 (2021) 1752–1766, https://doi.org/10.1016/S1872-5813(21)60135-4.
[15] A. Racha, C. Samanta, S. Sreekantan, B. Marimuthu, Review on catalytic hydrogenation of biomass-derived furfural to furfuryl alcohol: Recent advances and future trends, Energy Fuels 37 (2023) 11475–11496, https://doi.org/10.1021/acs.energyfuels.3c01174.
[16] G.K. Chuah, S. Jaenicke, Y.Z. Zhu, S.H. Kiu, Meerwein-Ponndorf-Verley reduction over heterogeneous catalysts, Curr. Org. Chem. 10 (2006) 1639–1654, https://doi.org/10.2174/138527206778249621.
[17] J.R. Ruíz, C. Jiménez-Sanchidrian, Heterogeneous catalysis in the Meerwein-Ponndorf-Verley reduction of carbonyl compounds, Curr. Org. Chem. 11 (2007) 1113–1125, https://doi.org/10.2174/138527207781662500.
[18] T. Komanoya, K. Nakajima, M. Kitano, M. Hara, Synergistic catalysis by Lewis acid and base sites on ZrO_2 for meerwein–ponndorf–verley reduction, J. Phys. Chem. C. 119 (2015) 26540–26546, https://doi.org/10.1021/acs.jpcc.5b08355.
[19] W.N. Moulton, R.E.V. Atta, R.R. Ruch, Mechanism of the meerwein-ponndorf-verley reduction, J. Org. Chem. 26 (1961) 290–292, https://doi.org/10.1021/jo01061a002.
[20] E.D. Williams, K.A. Krieger, A.R. Day, The mechanism of the Meerwein-Ponndorf -Verley reaction. A deuterium tracer study, J. Am. Chem. Soc. 75 (1952) 2404–2407, https://doi.org/10.1021/ja01106a037.
[21] C.F. de Graauw, J.A. Peters, H. van Bekkum, J. Huskens, Meerwein-ponndorf-verley reductions and oppenauer oxidations: an integrated approach, Synthesis (10) (1994) 1007–1017, https://doi.org/10.1055/s-1994-25625.
[22] K. Krohn, B. Knauer, The diastereoselectivity of zirconium alkoxide catalysed Meerwein-Ponndorf-Verley reductions, Liebigs Ann. (1995) 1347–1351, https://doi.org/10.1002/jlac.1995199507179.
[23] M.S. Kim, F.S.H. Simanjuntak, S. Lim, J. Jae, J.M. Ha, H. Lee, Synthesis of alumina-carbon composite material for the catalytic conversion of furfural to furfuryl alcohol, J. Ind. Eng. Chem. 52 (2017) 59–65, https://doi.org/10.1016/j.jiec.2017.03.024.
[24] R. López-Asensio, J.A. Cecilia, C.P. Jiménez-Gómez, C. García-Sancho, R. Moreno-Tost, P. Maireles-Torres, Selective production of furfuryl alcohol from furfural by catalytic transfer hydrogenation over commercial aluminas, Appl. Catal. A: Gen. 556 (2018) 1–9, https://doi.org/10.1016/j.apcata.2018.02.022.
[25] C. García-Sancho, C.P. Jiménez-Gómez, N. Viar-Antuñano, J.A. Cecilia, R. Moreno-Tost, J.M. Mérida-Robles, J. Requies, P. Maireles-Torres, Evaluation of the ZrO_2/Al_2O_3 system as catalysts in the catalytic transfer hydrogenation of furfural to obtain furfuryl alcohol, Appl. Catal. A: Gen. 609 (2021) 117905, https://doi.org/10.1016/j.apcata.2020.117905.
[26] V. Montes, J.F. Miñambres, A.N. Khalilov, M. Boutonnet, J.M. Marinas, F. J. Urbano, A.M. Maharramov, A. Marinas, Chemoselective hydrogenation of furfural to furfuryl alcohol on ZrO_2 systems synthesized through the microemulsion method, Catal. Today 306 (2018) 89–95, https://doi.org/10.1016/j.cattod.2017.05.022.
[27] J. Zhang, K. Dong, W. Luo, H. Guan, Selective transfer hydrogenation of furfural into furfuryl alcohol on Zr-containing catalysts using lower alcohols as hydrogen donors, ACS Omega 3 (2018) 6206–6216, https://doi.org/10.1021/acsomega.8b00138.
[28] Y. Zhang, Y. Cao, C. Yan, W. Liu, Y. Chen, W. Guan, F. Wang, Y. Liu, P. Huo, Rationally designed Au-ZrO_x interaction for boosting 5-hydroxymethylfurfural oxidation, Chem. Eng. J. 459 (2023) 141644, https://doi.org/10.1016/j.cej.2023.141644.
[29] Y. Zhang, Y. Liu, W. Guan, M. Cao, Y. Chen, P. Huo, Strong metal-support interaction between AuPd nanoparticles and oxygen-rich defect ZrO_2 for enhanced catalytic 5-hydroxymethylfurfural oxidation, Chin. Chem. Lett. 35 (2024) 108932, https://doi.org/10.1016/j.cclet.2023.108932.
[30] K.S. Koppadi, R.R. Chada, S.S. Enumula, R.K. Marella, S.R.R. Kamaraju, D.R. Burri, Metal-free hydrogenation of biomass derived furfural into furfuryl alcohol over carbon–MgO catalysts in continuous mode, Catal. Lett. 147 (2017) 1278–1284, https://doi.org/10.1007/s10562-017-2035-3.
[31] J. Hidalgo-Carrillo, A. Parejas, M.J. Cuesta-Rioboo, A. Marinas, F.J. Urbano, MPV reduction of furfural to furfuryl alcohol on Mg, Zr, Ti, Zr–Ti, and Mg–Ti solids: influence of acid-base properties, Catalysts 8 (2018) 539, https://doi.org/10.3390/catal8110539.
[32] R. López-Asensio, J.A. Cecilia-Buenestado, C. Herrera-Delgado, M.A. Larrubia-Vargas, C. García-Sancho, P.J. Maireles-Torres, R. Moreno-Tost, Mixed oxides derived from hydrotalcites Mg/Al active in the catalytic transfer hydrogenation of furfural to furfuryl alcohol, Catalysts 13 (2023) 45, https://doi.org/10.3390/catal13010045.
[33] L. Bui, H. Luo, W.R. Gunther, Y. Román-Leshkov, Domino reaction catalyzed by zeolites with Brønsted and Lewis acid sites for the production of γ-valerolactone from furfural, Angew. Chem. Int. Ed. 52 (2013) 8022–8025, https://doi.org/10.1002/anie.201302575.
[34] M.J. Gilkey, B. Xu, Heterogeneous catalytic transfer hydrogenation as an effective pathway in biomass upgrading, ACS Catal. 6 (2016) 1420–1436, https://doi.org/10.1021/acscatal.5b02171.
[35] M. Boronat, A. Corma, M. Renz, Mechanism of the Meerwein-Ponndorf-Verley-Oppenauer (MPVO) redox equilibrium on Sn- and Zr-beta zeolite catalysts, J. Phys. Chem. B 110 (2006) 21168–21174, https://doi.org/10.1021/jp063249x.
[36] M.M. Antunes, S. Lima, P. Neves, A.L. Magalhães, E. Fazio, A. Fernandes, F. Neri, C. M. Silva, S.M. Rocha, M.F. Ribeiro, M. Pillinger, A. Urakawa, A.A. Valente, One-pot conversion of furfural to useful bio-products in the presence of a Sn,Al-containing zeolite beta catalyst prepared via post-synthesis routes, J. Catal. 329 (2015) 522–537, https://doi.org/10.1016/j.jcat.2015.05.022.
[37] B. Tang, S. Li, W.C. Song, E.C. Yang, One-pot transformation of furfural into γ-valerolactone catalyzed by a hierarchical Hf-Al-USY zeolite with balanced Lewis and Brønsted acid sites, Sustain. Energy Fuels 5 (2021) 4724–4735, https://doi.org/10.1039/D1SE00942G.
[38] J.A. Melero, G. Morales, J. Iglesias, M. Paniagua, C. Lopez-Aguado, Rational optimization of reaction conditions for the one-pot transformation of furfural to γ-valerolactone over Zr–Al-beta zeolite: toward the efficient utilization of biomass, Ind. Eng. Chem. Res. 57 (2018) 11592–11599, https://doi.org/10.1021/acs.iecr.8b02475.
[39] K.D. Kim, J. Kim, W.Y. Teoh, J.C. Kim, J. Huang, R. Ryoo, Cascade reaction engineering on zirconia-supported mesoporous MFI zeolites with tunable Lewis–Brønsted acid sites: a case of the one-pot conversion of furfural to γ-valerolactone, RSC Adv. 10 (2020) 35318–35328, https://doi.org/10.1039/D0RA06915A.
[40] H.P. Winoto, B.S. Ahn, J. Jae, Production of γ-valerolactone from furfural by a single-step process using Sn-Al-Beta zeolites: Optimizing the catalyst acid properties and process conditions, J. Ing. Eng. Chem. 40 (2016) 62–71, https://doi.org/10.1016/j.jiec.2016.06.007.
[41] R. Barakov, N. Shcherban, O. Petrov, D.N. Rainer, M. Kubů, J. Čejka, M. Shamzhy, M. Opanasenko, Optimization of Zr-Al-USY and Zr-Al-Beta zeolites catalysts for a one-pot cascade transformation of furfural to γ-valerolactone, Catal. Today 426 (2024) 114406, https://doi.org/10.1016/j.cattod.2023.114406.
[42] A. García, R. Sánchez-Tovar, P.J. Miguel, E. Montejano-Nares, F. Ivars-Barceló, J. A. Cecilia, B. Torres-Olea, B. Solsona, Catalytic production of γ-valerolactone, a biofuel precursor, from furfural in one-pot: Synergistic effect between Zr and Sn, Fuel 352 (2023) 129045, https://doi.org/10.1016/j.fuel.2023.129045.
[43] Z. Liu, Z. Zhang, R. Fu, J. Xu, J. Lu, Z. Wen, B. Xue, One-pot conversion of furfural to gamma-valerolactone over Zr-SBA-15: Cooperation of Lewis and Brønsted acidic sites, ACS Appl. Nano Mater. 6 (2023) 13196–13207, https://doi.org/10.1021/acsanm.3c01845.
[44] J. Iglesias, J.A. Melero, G. Morales, M. Paniagua, B. Hernández, A. Osatiashtiani, A. F. Lee, K. Wilson, ZrO_2-SBA-15 catalysts for the one-pot cascade synthesis of GVL from furfural, Catal. Sci. Technol. 8 (2018) 4485–4493, https://doi.org/10.1039/C8CY01121D.
[45] J. Zhang, Y. Liu, S. Yang, J. Wei, L. He, L. Peng, X. Tang, Y. Ni, Highly selective conversion of furfural to furfural alcohol or levulinate ester in one pot over ZrO_2@SBA-15 and its kinetic behavior, ACS Sustain. Chem. Eng. 8 (2020) 5584–5594, https://doi.org/10.1021/acssuschemeng.9b07512.
[46] A. García, P.J. Miguel, A. Ventimiglia, N. Dimitratos, B. Solsona, Optimization of the Zr-loading on siliceous support catalysts leads to a suitable Lewis/Brønsted acid

sites ratio to produce high yields to γ-valerolactone from furfural in one-pot, Fuel 324 (2022) 124549, https://doi.org/10.1016/j.fuel.2022.124549.
[47] J. He, H. Li, Y. Xu, S. Yang, Dual acidic mesoporous KIT silicates enable one-pot production of γ-valerolactone from biomass derivatives via cascade reactions, Renew. Energy 146 (2020) 359–370, https://doi.org/10.1016/j.renene.2019.06.105.
[48] R. Maderuelo-Solera, S. Richter, C.P. Jiménez-Gómez, C. García-Sancho, F. J. García-Mateos, J.M. Rosas, R. Moreno-Tost, J.A. Cecilia, P. Maireles-Torres, Porous SiO_2 nanospheres modified with ZrO_2 and their use in one-pot catalytic processes to obtain value-added chemicals from furfural, Ind. Eng. Chem. Res. 60 (2021) 18791–18805, https://doi.org/10.1021/acs.iecr.1c02848.
[49] P. Zhang, P. Hou, M. Ma, K. Bu, Q. Guo, H. Yue, G. Tian, S. Feng, Bifunctional zirconium-based metal-organic frameworks as chemoselective catalysts for the synthesis of γ-valerolactone from furfural via a one-pot cascade reaction, Appl. Catal. A: Gen. 653 (2023) 119064, https://doi.org/10.1016/j.apcata.2023.119064.
[50] A.H. Valekar, M. Lee, J.W. Yoon, J. Kwak, D.Y. Hong, K.R. Oh, G.Y. Cha, Y. U. Kwon, J. Jung, J.S. Chang, Y.K. Hwang, Catalytic transfer hydrogenation of furfural to furfuryl alcohol under mild conditions over Zr-MOFs: Exploring the role of metal node coordination and modification, ACS Catal. 10 (2020) 3720–3732, https://doi.org/10.1021/acscatal.9b05085.
[51] J.M. Guarinos, F.G. Cirujano, A. Rapeyko, F.X. Llabrés i Xamena, Conversion of levulinic acid to γ-valerolactone over Zr-containing metal-organic frameworks: Evidencing the role of Lewis and Brønsted acid sites, Mol. Catal. 515 (2021) 111925, https://doi.org/10.1016/j.mcat.2021.111925.
[52] X. Xia, H. Yu, P. Qin, M. Dai, L. Jia, Y. Deng, C. Li, F. Li, Organodiphosphonate Zr-MOF: A highly efficient catalyst for Meerwein–Ponndorf–Verley reduction of furfural, Asia-Pac. J. Chem. Eng. 18 (2023) e2937, https://doi.org/10.1002/apj.2937.
[53] A. García, E. Monti, A. Ventimiglia, N. Dimitratos, P.J. Miguel, M.L. López, I. Álvarez-Serrano, T. García, M.P. Pico, A.M. Dejoz, B. Solsona, Zr supported on non-acidic sepiolite for the efficient one-pot transformation of furfural into γ-valerolactone, Biomass-.-. Bioenergy 170 (2023) 106730, https://doi.org/10.1016/j.biombioe.2023.106730.
[54] S. Essih, J.A. Cecilia, C.P. Jiménez-Gómez, C. García-Sancho, F.J. García-Mateos, J. M. Rosas, R. Moreno-Tost, F. Franco, P. Maireles-Torres, Synthesis of porous clay heterostructures modified with SiO_2–ZrO_2 nanoparticles for the valorization of furfural in one-pot process, Adv. Sustain. Syst. 6 (2022) 2100453, https://doi.org/10.1002/adsu.202100453.
[55] T. Zhang, Y. Lu, W. Li, M. Su, T. Yang, A. Ogunbiyi, Y. Jin, One-pot production of γ-valerolactone from furfural using Zr-graphitic carbon nitride/H-β composite, Int. J. Hydrog. Energy 44 (2019) 14527–14535, https://doi.org/10.1016/j.ijhydene.2019.04.059.
[56] J.M. Rosas, J. Bedia, J. Rodríguez-Mirasol, T. Cordero, On the preparation and characterization of chars and activated carbons from orange skin, Fuel Process. Technol. 91 (2010) 1345–1354, https://doi.org/10.1016/j.fuproc.2010.05.006.
[57] J.M. Rosas, J. Bedia, J. Rodríguez-Mirasol, T. Cordero, HEMP-derived activated carbon fibers by chemical activation with phosphoric acid 88 (2009) 19–26, https://doi.org/10.1016/j.fuel.2008.08.004.
[58] V. Torres-Bujalance, J.A. Cecilia, C. García-Sancho, F.J. García-Mateos, J.M. Rosas, R. Moreno-Tost, J. Rodríguez-Mirasol, T. Cordero, P. Maireles-Torres, Valorization of olive stones for the synthesis of phosphorus-modified porous carbons and their use as support of Pd particles for the oxidative condensation of furfural with ethanol, Renew. Energy 221 (2024) 119772, https://doi.org/10.1016/j.renene.2023.119772.
[59] M. Thommes, K. Kaneko, A.V. Neimark, J.P. Olivier, F. Rodríguez-Reinoso, J. Rouquerol, K.S.W. Sing, Physisorption of gases, with special reference to the evaluation of surface area and pore size distribution (IUPAC Technical Report), Pure Appl. Chem. 87 (2015) 1051–1069, https://doi.org/10.1515/pac-2014-1117.
[60] Z.Q. Li, C.J. Lu, Z.P. Xia, Y. Zhou, Z. Luo, X-ray diffraction patterns of graphite and turbostratic carbon, Carbon 45 (2007) 1686–1695, https://doi.org/10.1016/j.carbon.2007.03.038.
[61] F. Tuinstra, J.L. Koenig, Raman spectrum of graphite, J. Chem. Phys. 53 (1970) 1126–1130, https://doi.org/10.1063/1.1674108.
[62] N. Chouikhi, J.A. Cecilia, E. Vilarrasa-García, L. Serrano-Cantador, S. Besghaier, M. Chlendi, M. Bagane, E.Rodríguez Castellón, Valorization of agricultural waste as a carbon materials for selective separation and storage of CO_2, H_2 and N_2, Biomass-.-. Bioenergy 155 (2021) 106297, https://doi.org/10.1016/j.biombioe.2021.106297.
[63] J.A. Cecilia, E. Vilarrasa-García, N. Chouikhi, R. Morales-Ospino, S. Besghaier, M. Chlendi, M. Bagane, M. Bastos-Neto, D.C.S. Azevedo, E. Rodríguez-Castellón, Activated carbons synthesized from sucrose using porous clay heterostructures as template for CO_2 adsorption, Sustain. Chem. Clim. Action 1 (2022) 100006, https://doi.org/10.1016/j.scca.2022.100006.
[64] R.J. Nemanich, S.A. Dolin. First- and second-order Raman scattering from finitesize crystals of graphite, Phys. Rev. B 20 (1979) 392–401, https://doi.org/10.1103/PhysRevB.20.392.
[65] A.C. Ferrari, D.M. Basko, Raman spectroscopy as a versatile tool for studying the properties of graphene, Nat. Nanotechnol. 8 (2013) 235–246, https://doi.org/10.1038/nnano.2013.46.
[66] A.M. Puziy, O.I. Poddubnaya, R.P. Socha, J. Gurgul, M. Wisniewski, XPS and NMR studies of phosphoric acid activated carbons, Carbon 46 (2008) 2113–2123, https://doi.org/10.1016/j.carbon.2008.09.010.
[67] M.J. Valero-Romero, F.J. García-Mateos, J. Rodríguez-Mirasol, T. Cordero, Role of surface phosphorus complexes on the oxidation of porous carbons, Fuel Process. Technol. 157 (2017) 116–126, https://doi.org/10.1016/j.fuproc.2016.11.014.
[68] R. López-Asensio, C.P. Jiménez Gómez, C. García Sancho, R. Moreno-Tost, J. A. Cecilia, P. Maireles-Torres, Influence of structure-modifying agents in the synthesis of Zr-doped SBA-15 silica and their use as catalysts in the furfural hydrogenation to obtain high value-added products through the Meerwein-Ponndorf-Verley reduction, Int. J. Mol. Sci. 20 (2019) 828, https://doi.org/10.3390/ijms20040828.
[69] E. Selli, L. Forni, Comparison between the surface acidity of solid catalysts determined by TPD and FTIR analysis of pre-adsorbed pyridine, Microporous Mesoporous Mater. 31 (1999) 129–140, https://doi.org/10.1016/S1387-1811(99)00063-3.
[70] C. Morterra, G. Cerrato, G. Meligrana, Revisiting the use of 2,6-dimethylpyridine adsorption as a probe for the acidic properties of metal oxides, Langmuir 17 (2001) 7053–7060, https://doi.org/10.1021/la010707e.
[71] L. Faba, E. Díaz, S. Ordoñez, Aqueous-phase furfural-acetone aldol condensation over basic mixed oxides, Appl. Catal. B: Environ. 113 (2012) 201–211, https://doi.org/10.1016/j.apcatb.2011.11.039.
[72] G. Morales, M. Paniagua, D. de la Flor, M. Sanz, P. Leo, C. López-Aguado, H. Hernando, S.A. Orr, K. Wilson, A.F. Lee, J.A. Melero, Aldol condensation of furfural and methyl isobutyl ketone over Zr-MOF-808/silica hybrid catalysts, Fuel 339 (2023) 127465, https://doi.org/10.1016/j.fuel.2023.127465.
[73] Y. Xu, X. Liu, H. Guo, M. Qiu, X. Qi, Efficient catalytic transfer hydrogenation of furfural to furfuryl alcohol over Zr-doped ordered mesoporous carbon synthesized by Zr-arbutin coordinated self-assembly, Fuel 331 (2023) 125834, https://doi.org/10.1016/j.fuel.2022.125834.
[74] R. Maderuelo-Solera, R. López-Asensio, J.A. Cecilia, C.P. Jiménez-Gómez, C. García-Sancho, R. Moreno-Tost, P. Maireles-Torres, Catalytic transfer hydrogenation of furfural to furfuryl alcohol over calcined MgFe hydrotalcites, Appl. Clay Sci. 183 (2019) 105351, https://doi.org/10.1016/j.clay.2019.105351.